EUROFUSION WPMST2-PR(16) 14814

R Dejarnac et al.

Power loads to misaligned edges in COMPASS

Preprint of Paper to be submitted for publication in
22nd International Conference on Plasma Surface Interactions
in Controlled Fusion Devices (22nd PSI)

This work has been carried out within the framework of the EUROfusion Consortium and has received funding from the Euratom research and training programme 2014-2018 under grant agreement No 633053. The views and opinions expressed herein do not necessarily reflect those of the European Commission.

Power deposition on misaligned edges in COMPASS

R. Dejarnac[a,*], Y. Corre[b], P. Vondracek[a], J-L. Gardarein[c], J. Gaspar[c], E. Gauthier[b], J. P. Gunn[b], J. Horacek[a], M. Hron[a], M. Komm[a], R. Panek[a], R. A. Pitts[d] and the COMPASS team

[a]*Institute of Plasma Physics, Czech Academy of Sciences, 182 00 Prague, Czech Republic*
[b]*CEA, IRFM, F-13108 Saint-Paul-lez-Durance, France*
[c]*Université d'Aix-Marseille, CNRS, IUSTI UMR 7343, F-13013 Marseille, France*
[d]*ITER Organisation, CS 90 046, F-13067 St Paul-lez-Durance cedex, France*

[*]*corresponding author: Renaud Dejarnac dejarnac@ipp.cas.cz*

Abstract
If the decision is made not to apply a toroidal chamfer to tungsten monoblocks at ITER divertor vertical targets, exposed leading edges will arise as a result of assembly tolerances between adjacent plasma-facing components. Then, the advantage of glancing magnetic field angles for spreading plasma heat flux on top surfaces is lost at the misaligned edges with an interaction occurring at near normal incidence, which can drive melting for the expected inter-ELM heat fluxes. A dedicated experiment has been performed on the COMPASS tokamak to thoroughly study power deposition on misaligned edges using inner-wall limited discharges on a special graphite tile presenting gaps and leading edges directly viewed by a high resolution infra-red camera. The parallel power flux deducted from the unperturbed measurement far from the gap is fully consistent with the observed temperature increase at the leading edge, respecting the power balance. All the power flowing into the gap is deposited at the leading edge and no mitigation factor is required to explain the thermal response. Particle-in-cell simulations show that the ion Larmor smoothing effect is weak and that the power deposition on misaligned edges is well described by the optical approximation because of an electron dominated regime associated with non-ambipolar parallel current flow.

1. Introduction

The ITER full tungsten (W) divertor targets will be castellated to withstand thermo-mechanical stress and made of ~300 000 independent monoblocks separated by 0.4-to-3.5 mm gaps with a mechanical assembly tolerance between adjacent plasma-facing components (PFCs) of ~0.3 mm [1]. Consequently, the presence of leading edges (LEs) in the present design is inevitable and represents a major issue for the future ITER operation. The advantage of glancing magnetic field angles (~3° at the ITER divertor targets) for spreading plasma heat flux on top surfaces is lost at the misaligned edges with an interaction occurring at near normal incidence, which can quickly drive melting of W for the inter-ELM heat fluxes expected in ITER. In order to understand power loading in the case of small-scale exposed edges, the fusion community has directed considerable effort into numerical modeling [2,3] and dedicated experiments [4]. Geometrical arguments assume that power loads on the top and side of a leading edge may be described by $Q_n = q_{//,0}*\sin(\alpha)$ and $Q_s = q_{//,0}*\cos(\alpha)$, respectively, with $q_{||,0}$ the heat flux density parallel to B and α the field line angle. This optical approximation (OA) assumption has, however, recently been challenged by edge melting experiments on JET [5], which found that the theoretically expected Q_s on the side of the LE needed to be reduced by a factor 5 in L-mode plasmas to explain the observed power load, whilst Q_n was as expected, thus violating the power balance. Such discrepancies are a significant issue for ITER as it still considers the option of shaping divertor monoblocks. Therefore, as part of a coordinated ITPA effort, a dedicated experiment has been designed on COMPASS to thoroughly study this phenomenon.

A special graphite tile with four recessed regions in order to create LEs, which are separated by poloidal gaps (PGs) has been installed on the COMPASS inner wall at a location viewed directly by a high resolution infra-red (IR) camera. Different misalignments ($0 < h < 0.9\ mm$) are chosen for each region covering both the typical maximum misalignment (~0.3 mm) expected on ITER and the value used in the JET experiment (~1.0 mm). Moreover, one LE region presents a recessed volume to exactly recreate the JET melting set-up, where several lamellas before the protruding lamella were recessed to avoid any shadowing [5]. One of the hypotheses to explain the JET strong mitigation was a possible perturbation of the local plasma in front of the lamella by the creation of a mini scrape-off layer (SOL). Ohmically heated, inner wall limited discharges in the COMPASS tokamak are used with ITER relevant incident angles $\alpha = 2.5^{o}$ on the test tile. Technical details of this experiment are given in Section 2. The surface temperature distribution on the inner-wall limiter (IWL) is calculated by 2D thermal simulations based on the finite element method. The methodology used to compare experimental IR data with simulation results is explained in Section 3. The power deposition profiles around the different PGs and LEs are calculated by a 2D particle-in-cell (PIC) code. The synthetic surface temperature profiles from thermal simulations using as input the power deposition profiles from 1) the OA and 2) the PIC calculations are compared to experimental IR data and results are presented in Section 4. Finally, the main conclusions are summarized in Section 5.

2. Experimental set-up on COMPASS

2.1. The COMPASS IWL

The heat loads on misaligned edges are investigated using a dedicated IWL, specially designed to present ITER relevant LE heights and incident angles between the field lines and the top surface, see Fig. 1. The set-up is similar to the one used in [6,7] to study the narrow SOL power flux component in limiter discharges. The IWL is made of graphite and has a roof-shape with an apex in the middle protruding by 6 mm above the two toroidal neighbouring panels. The COMPASS inner-wall is made of 32 panels separated by 2 mm gaps. The IWL is 133 mm wide toroidally, representing two standard panels with a toroidal expansion of 22.5°. The slope of each side makes a 2.5° angle with respect to the last closed flux surface (LCFS) defined at the apex. The central tile (90 mm long in the poloidal direction, z) includes four regions, with each region presenting a poloidally running gap and a LE with a fixed misalignment, h. The PG ($l^{gap} = 1$ mm) is located in the middle of each side allowing a comfortable 30 mm unperturbed region downstream the LE towards the apex for good IR measurements. The misalignment is

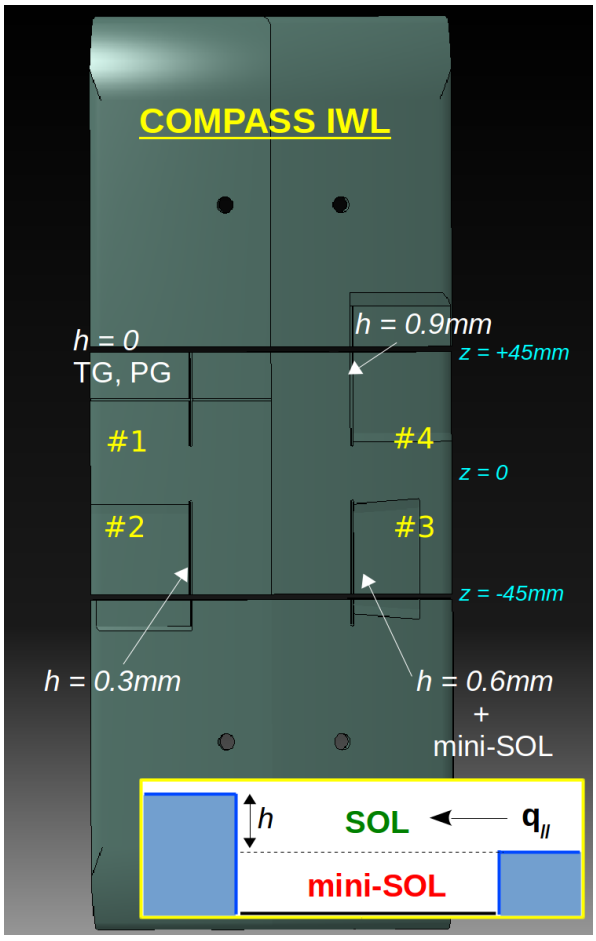

Figure 1: Schematic view of the COMPASS IWL with the 4 regions equipped with gaps and LEs. The inset shows the detail of the mini-SOL concept.

different for each region, *h = 0, 0.3, 0.6, 0.9 mm* anti-clockwise from region #1, covering both the typical maximum misalignment (~0.3 mm) expected on ITER in region #2 and the value used in the JET experiment (~1.0 mm) in region #4. In order to recreate the JET experimental set-up [5], where 8 lamellas before the protruding lamella were recessed to avoid any shadowing, the region #3 presents a closed pocket before the LE to develop a mini-SOL (see Fig. 1). Additionally, we know by experience on COMPASS that the limiter is prone to tilting around the apex vertical axis when installing it on the central column. In order to determine the tilt with high precision, the IWL bottom tile has been designed rounded with a curvature radius half the tokamak major radius. Consequently, the perpendicular power flux toroidal profile along this tile should present a minimum when the field lines are tangential, $\alpha = 0^{o}$. In this rounded configuration, the inclination varies linearly with the toroidal distance by 1^{o} every 12 mm. The power flux density perpendicular to the surface is calculated from IR measurements using the 2D heat transfer code THEODOR [8]. Six IWL discharges with the contact point on the bottom tile show similar positions of the perpendicular flux minimum, shifted left from the apex by 12 mm, yielding a tilt of $+1^{o}$. The inclination between the magnetic field lines and the IWL surfaces is therefore 1.5^{o} on the left side and 3.5^{o} on the right side.

2.2. The IR thermography system and plasma scenario

The COMPASS IWL is monitored by a mid-IR InSb camera with a 240x320 pixel resolution mounted on an outer mid-plane port directly viewing the limiter. The 100 mm lens mounted on the camera yields a resolution *r = 0.3 mm/pixel* and a field of view corresponding to one enlarged region. In order to resolve the entire IWL central tile, a 50 mm lens is used giving *r = 0.5 mm/pixel*. Processed data give the surface temperature, $T^{surf,IR}$, toroidal profiles at the plasma contact point.

Ohmically heated and slightly elongated (elongation = 1.1) inner-wall limited deuterium discharges are used with $B_T = 0.9$ T and $I_p = 130$ kA, giving $Q_n \sim 1$ MWm^{-2} on the non-perturbed top surfaces far from the gaps. Discharges are typically ~300 ms long with a steady-state phase of ~150 ms. The plasma column leans on the IWL with the contact point at 2 different vertical positions on the central tile, z = +35 mm and z = -35 mm, intercepting the LEs of regions #1, #4 and regions #2, #3, respectively (see Fig. 1). Only the results from the latter regions will be presented here.

3. Methodology

In order to determine the true heat loads and temperature peaks around the gaps and LEs, a complete thermal modelling of the IWL coupled to a sensor correction technique [9] for direct comparison with experimental IR data ($T^{surf,IR}$) is performed and is briefly described in this section.

3.1. Heat load characterization

The power flux falling on the IWL is determined for each side of the limiter, which shadows each other due to the limiter geometry. The orientation of both B_T and I_p being in the standard direction clockwise, the left side corresponds to the electron side and receives in average parallel power loads ~25% higher than on the right side. However, due to the 1^{o} tilt of the limiter, the left side receives ~2 times lower perpendicular power than on the right side. Therefore, each side is treated separately for the heat load characterization. The surface temperature distribution on the IWL is retrieved from 2D finite element thermal calculations

using the code CAST3M [10]. The simulation input fluxes are determined in two steps. Firstly, Q_n is determined unambiguously on an unperturbed region downstream far from the gap to match the temperature there. Once Q_n is fixed (and will remain fixed for the rest of different procedures), Q_s is determined by iteration and minimization until a match is found with the experimental data at the LE corner. Due to the limiter geometry and the narrow power decay length (λ_q) in COMPASS IWL discharges [6,7], the radial exponential variation of the flux is taken into account. Moreover, the power from radiation (Q_{rad}), measured by bolometry, is subtracted from the perpendicular power flux when calculating Q_s in order to only have the convected flux. In the present experiment, $Q_{rad} \sim 0.20$ MW/m^2. Assuming the OA approach, the power flux along one IWL side is:

$$Q_s = (Q_n - Q_{rad})/sin(\alpha) * e^{(-dLCFS/\lambda q)} \quad (1)$$

with d_{LCFS} the radial distance from the LCFS.
Typical values for this experiment are $Q_n = 0.8$ MW/m^2, $Q_s = 16$ MW/m^2 on the left side and $Q_n = 1$ MW/m^2, $Q_s = 10$ MW/m^2 on the right side with $\lambda_q = 7$ mm.

3.2. The 2D thermal simulations

The OA power fluxes as determined in Section 3.1. are given as input of the thermal calculations and applied to the entire 2D geometry of each IWL side, providing the simulated surface temperature, $T^{surf,simul}$. The power flux profiles can also be taken from PIC calculations (see Section 4.2.). PIC profiles also present a constant perpendicular flux far from the gap/LE and are therefore normalised to the same Q_n as in the OA case. The profiles usually differ around the LE.

3.3. Synthetic IR data reconstruction

Around the LE corner, the temperature profile strongly increases with large gradients. The quantitative comparison between the code results, with its fine spatial mesh resolution, and the experimental IR data can thus be challenging. Indeed, the measurement smooths the real profiles by the IR camera optical line transfer function and by the detector transfer function due to its finite size for photon conversion. In order to compare the code output with the experimental IR data, numerical profiles are convoluted with a modulation transfer function specific to the camera [9]. This function is modelled by a Gaussian in the frequency space with a standard deviation being half of the IR camera spatial resolution. The resulting surface temperature is a synthetic reconstruction of what our camera should see, $T^{surf,synthetic}$, and a direct comparison can thus be performed. In the rest of the manuscript, all simulation output will be $T^{surf,synthetic}$.

4. Power deposition around leading edges

4.1. The optical approximation

The comparison between the experiment and the simulations using the OA ($T^{surf,OA}$) is done for the COMPASS discharge #11620 (*r = 0.5 mm/pixel*) with the plasma contact point covering both regions #2 and #3, see Fig. 2. A perfect qualitative and quantitative agreement is observed between $T^{surf,OA}$ and $T^{surf,IR}$ both on the temperature decay and at the peak for the two simulated LEs. The two pairs of (Q_n, Q_s) used in the two sides are consistent with the OA and done for the same $\lambda_q = 7$ mm using eq. (1). However, on the left side, where this effect is

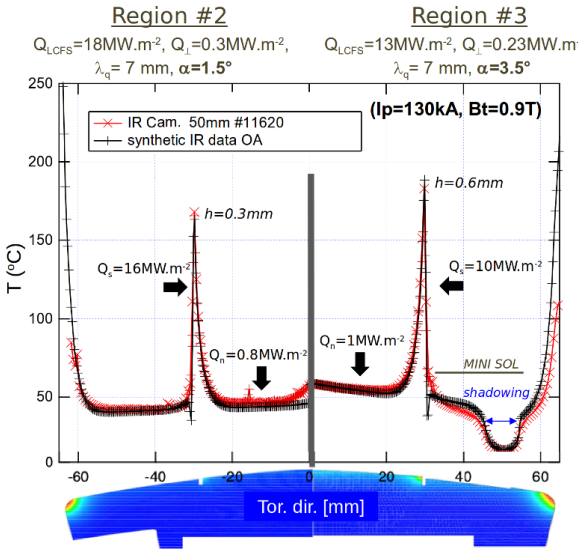

Figure 2: Experimental (x) and synthetic (+) T^{surf} profiles along the toroidal direction at z = -35 mm covering both regions #2 and #3.

stronger due to a shallower angle (1.5°), a perpendicular flux $Q_{\perp} = 0.3$ MW/m^2 > Q_{rad} has to be subtracted to Q_n in eq. (1) to match $T^{surf,IR}$. This is attributed to extra cross-field transport Q_{xf} at almost tangential inclination of the field lines [11,12]. Therefore, Q_{rad} has to be substituted by $Q_{\perp} = Q_{rad} + Q_{xf}$, in eq. (1). This perpendicular flux is not measured but arbitrarily fixed in order to match experimental data. On the other hand, the $Q_{\perp}$ value needed here matches exactly the minimum value from the THEDOR profile on the rounded IWL tile for a tangential contact and represents ~30% of Q_n. On region #3, the IR profile is well reproduced by the simulation despite the mini-SOL. The temperature drop due to the magnetic shadow in the mini-SOL is also well reproduced. The two main conclusions that we can draw from such results is that 1) the OA is a valid approach to describe the power deposition on small LEs with grazing incident angles and 2) the mini-SOL in front of the LE is not responsible for any Q_s mitigation in the present COMPASS experiment as it was observed in JET [5]. Indeed, no mitigation factors have to be applied in any case to the OA description of power fluxes around LEs to match $T^{surf,IR}$. The recessed volume before the misaligned edge does not affect the power falling on it.

4.2. The Larmor smoothing effect

The deposited power profiles around the LEs can be calculated by the 2D-3V PIC code [13] that was used for previous similar studies [3,14]. The code simulates the thin region of the collisionless electrostatic sheath forming around any PFC. It resolves the trajectories of ions and electrons in a self-consistent electric field, derived from the Poisson's equation. The potential drop in the sheath and pre-sheath is fixed to floating conditions at -3kT_e with respect to the plasma potential. Collisions are not taken into account and a completely absorbing, conducting wall is simulated. The choice of the PIC technique is relevant because the gap size (*1 mm*) and LEs heights ($h \leq 0.9$ *mm*) are comparable to the ion Larmor radius for the plasma conditions of the experiment. The input parameters (electron density, ion and electron temperatures) are based on Langmuir probe measurements done in a previous COMPASS IWL experiment with similar plasma parameters [6]. The values taken for the simulations are $n_e = 5.10^{18}$ m^{-3} and $T_i = T_e = 35$ eV, yielding an ion Larmor radius $r_L \sim 0.8$ mm.

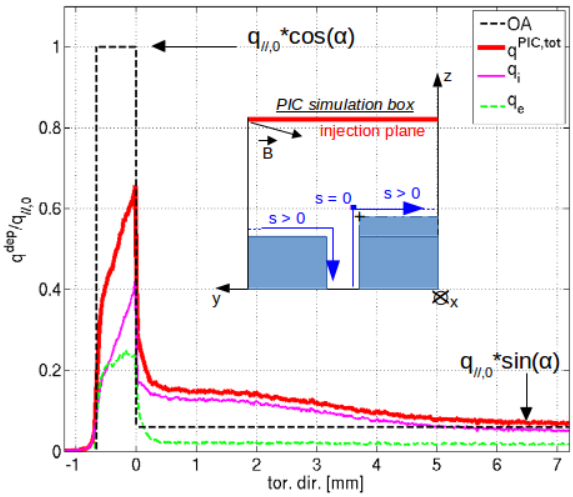

Figure 3: Deposited power flux around the 0.6 mm LE in region #3 calculated by PIC. The total flux (thick line) is composed of the ion (thin line) and electron (thin dots) contribution. The OA parallel flux (dashed) is indicated for comparison. The scheme of the PIC simulation box is shown in the inset with the s coordinate used to plot the toroidal profiles.

Based on PIC simulations, the power deposition profile around a LE differs from the OA when the misalignment height $h < 2r_L$ [15]. The incoming flux on the LE side is mitigated by a factor $f_s < 1$ with respect to $Q_s = q_{//,0}*\cos(\alpha)$ due to the Larmor smoothing effect, and the missing power is redeposited downstream on the LE top surface, thus enhancing there the theoretical flux $Q_n = q_{//,0}*\sin(\alpha)$ by a factor $f_n > 1$, respecting the power balance. The PIC power deposition profile normalised to the parallel flux around the 0.6 mm LE of region #3 is shown in Fig. 3. The OA flux is shown in dashed line for comparison. For this particular case, the simulation yields $f_s = 0.5$ and $f_n = 2.5$. The toroidal spreading of the redeposited power on the top surface (for $s > 0$) can be fitted by a Gaussian with $\sigma = 2.8$mm.

The consequent $T^{surf,PIC}$ profile is shown in Fig. 4. The profile using the OA is also plotted for comparison as well as $T^{surf,IR}$. It can be seen that $T^{surf,PIC}$ does not reproduce the experimental temperature. The discrepancy is twofold, 1) the predicted peak temperature at the LE corner is significantly lower and 2) the temperature decay is slower than the experimental one. It has to be noted that the analysis is not limited by the camera pixel size. These two points are a direct consequence of the shape of the total power deposition profile predicted by PIC, which is dominated by the contribution from the ions (see Fig. 3). Therefore, we can conclude that the ion Larmor smoothing effect is not a dominant effect in the power deposition process around small LEs. Therefore, the assumptions used in the code have to be questioned. The PIC model assumes a floating sheath and in this condition the fraction of the total power flux (q_{tot}) carried by ions (q_i) is dominant with respect to the one carried by electrons (q_e), which assumes the OA because of the very small electron Larmor radii, and can be expressed as $q_{tot} = f*q_i + (1-f)*q_e$, with $f = 5/7$ [16], as shown in Fig. 3. Experimental observations tend to show that the flux is governed by the OA or is more electron dominated. This can be the consequence of local electric currents and/or secondary electron emission, which would reduce the potential drop in the sheath. Langmuir probe measurements from a previous similar experiment [6] show a negative floating potential ~ $-1.5kT_e$ within 10 mm from the LFCS, where the LEs are

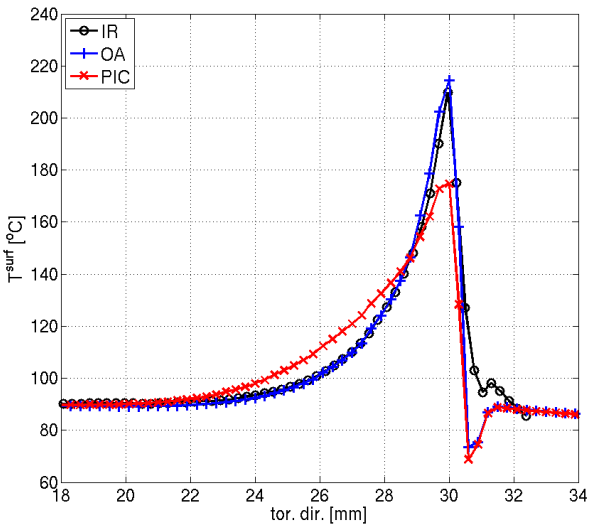

Figure 4: Experimental (o), OA (+) and PIC (x) T^{surf} profiles around the 0.6 mm LE in region #3.

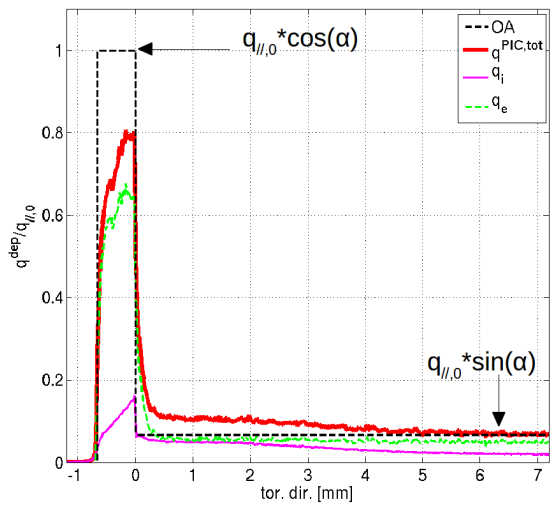

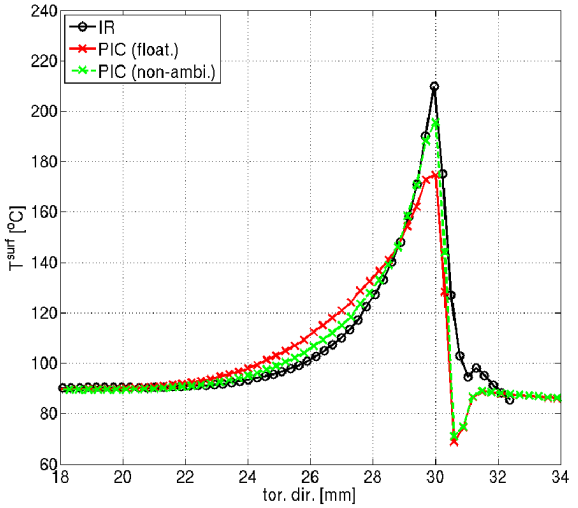

Figure 5: Deposited power flux around the 0.6 mm LE in region #3 calculated by PIC with non-ambipolar conditions and OA (left) and the consequent $T^{surf,PIC}$ profiles compared to $T^{surf,IR}$ (right).

located. This tells us that conditions near the LEs are not ambipolar and this should be taken into account in the PIC model. Using the PIC power flux profile from Fig. 3 but arbitrarily changing the contribution of ions and electrons by taking f = 2/7 changes the total power flux profile closer to the OA (see Fig. 5-left). The smoothing on the side is decreased ($f_s = 0.75$) and so is the redeposited missing power ($f_n = 1.7$). The consequence on the $T^{surf,PIC}$ can be seen in Fig. 5-right. The comparison with the floating case shows an improvement with a higher peak temperature at the corner, closer to the experimental one, and a better agreement of the decay, even if a slight discrepancy still remains. Further investigations should be performed, as implementing the real non-ambipolarity in the PIC code but also secondary electron emission.

5. Conclusions

This paper reports on dedicated experiments of heat loads on small misaligned edges in the COMPASS tokamak. A specially designed IWL was equipped with PGs and LEs of comparable sizes than the ion Larmor radii (< 1 mm), intersecting the magnetic field lines at grazing incidence ($1.5^o \leq \alpha \leq 3.5^o$). The limiter is in a direct view of a high resolution IR camera (0.3 mm/pixel). The experimental $T^{surf,IR}$ profiles are compared to the ones from 2D finite element calculations using as input the power flux profiles from either the geometric OA or PIC simulations. The main result shows that all measurements around all the different LEs (*h = 0, 0.3, 0.6, 0.9 mm*) are reproduced by the OA. One of the COMPASS IWL region (*h = 0.6 mm*) is equipped with a recessed volume before the LE to recreate the mini-SOL configuration of the 2013 JET experiment, which was a candidate to explain the strong mitigation of the parallel flux [5]. In COMPASS, no mitigation at all is needed to reproduce experimental data with the OA, thus ruling out the mini-SOL hypothesis. However, when applying the OA, a cross-field transport of order ~30% Q_n, consistent with experimental observations, has to be taken into account, especially at grazing angle $\leq 1.5^o$, where this effect is more pronounced. Within this condition, we can conclude that the OA is a valid approach for calculating the power deposition around small LEs.
Power deposition profiles around LEs in PGs from PIC calculations show a smoothing of the power on the LE side due to the ion Larmor gyration and a downstream enhanced flux on the LE top, toroidally spread, conserving the power balance. For a small LE (*h = 0.6 mm*) and under the assumption of ambipolarity implemented in the PIC code, the predicted power flux profiles do not match the IR measurements. The peak temperature at the LE corner is significantly lower and the temperature decay is slower than the experimental one. This result tends to show that the power is not dominated by ions but more by electrons. Arbitrary changing the composition of the total power profile in order to have most power carried by electrons show a better agreement with experimental data. Such an effect is consistent with a smaller potential drop in the sheath than assumed in the code, which is consistent with Langmuir probe measurements showing a negative floating potential at the LEs locations. Local electric currents seem to play a large role in the power distribution around small LEs into gaps and should be further investigated.

Acknowledgement
This work has been performed under EUROfusion WP PFC. It has been co-funded by MEYS projects number 8D15001 and LM2015045. This work has been carried out within the framework of the EUROfusion Consortium and has received funding from the Euratom research and training programme 2014-2018 under grant agreement No 633053. The views and opinions expressed herein do not necessarily reflect those of the European Commission.

References

[1] S Carpentier-Chouchana et al., *Phys. Scr.* **T159** (2014) 014002.
[2] J P Gunn et al., *this conference I-7*.
[3] M Komm et al., *this conference, P2-83*.
[4] R A Pitts et al., *this conference, I-6.*
[5] J W Coenen et al., *Nucl. Fusion* **55** (2015) 023010.
[6] R Dejarnac et al., *J. of Nucl. Mater.* **463** (2015) 381-384.
[7] J Horacek et al., *J. of Nucl. Mater.* **463** (2015) 385-388.
[8] A Herrmann, *Plasma Phys. Contr. Fusion* **37** (1995) 17.
[9] Y Corre et al., *submitted to Nucl. Fusion*.
[10] P Verpaux et al., *CASTEM 2000: a modern approach of computerized structural analysis*, Risley, UK (1988).
[11] G F Matthews et al., *Plasma Phys. Contr. Fusion* **32** (1991) 1301.
[12] Y Corre et al., *J. of Nucl. Mater.* **463** (2015) 832-836.
[13] R Dejarnac and J P Gunn, *J. of Nucl. Mater.* **363-365** (2007) 560-564.
[14] R Dejarnac et al., *Nucl. Fusion* **54** *(2014)* 123011.
[15] R Dejarnac et al., *J. Nucl. Mater.* **415** (2011) p. S977-S980.
[16] P C Stangeby, *The plasma boundary of magnetic fusion devices*, IoP Publishing Ltd.